

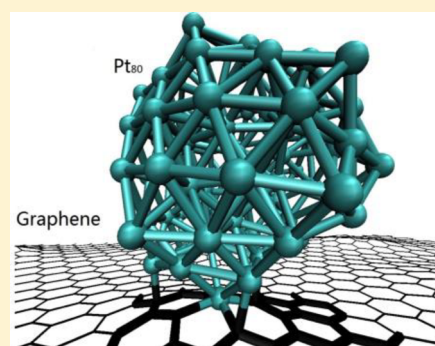
First-Principles Predictions of Structure–Function Relationships of Graphene-Supported Platinum Nanoclusters

Hongbo Shi,[†] Scott M. Auerbach,^{*,†,‡} and Ashwin Ramasubramaniam^{*,§}

[†]Department of Chemical Engineering, [‡]Department of Chemistry, and [§]Department of Mechanical and Industrial Engineering, University of Massachusetts Amherst, Amherst, Massachusetts 01003, United States

Supporting Information

ABSTRACT: Platinum-based materials play an important role as electrocatalysts in energy conversion technologies. Graphene-supported Pt nanoclusters were recently found to be promising electrocatalysts for fuel-cell applications due to their enhanced activity and tolerance to CO poisoning as well as their long-term stability toward sintering. However, structure–function relationships that underpin the improved performance of these catalysts are still not well understood. Here, we employ a combination of empirical potential simulations and density functional theory (DFT) calculations to investigate structure–function relationships of small Pt_N (N = 2–80) clusters on model carbon (graphene) supports. A bond-order empirical potential is employed within a genetic algorithm to go beyond local optimizations in obtaining minimum-energy structures of Pt_N clusters on pristine as well as defective graphene supports. Point defects in graphene strongly anchor Pt clusters and also appreciably affect the morphologies of small clusters, which are characterized via various structural metrics such as the radius of gyration, average bond length, and average coordination number. A key finding from the structural analysis is that the fraction of potentially active surface sites in supported clusters is maximized for stable Pt clusters in the size range of 20–30 atoms, which provides a useful design criterion for optimal utilization of the precious metal. Through selected *ab initio* studies, we find a consistent trend for charge transfer from small Pt clusters to defective graphene supports resulting in the lowering of the cluster d-band center, which has implications for the overall activity and poisoning of the catalyst. The combination of a robust empirical potential-based genetic algorithm for structural optimization with *ab initio* calculations opens up avenues for systematic studies of supported catalyst clusters at much larger system sizes than are accessible to purely *ab initio* approaches.



1. INTRODUCTION

Platinum clusters and nanoparticles are widely used as electrocatalysts and play an important role in the development of clean energy technologies such as hydrogen-based or methanol-based proton-exchange membrane fuel cells.^{1–3} Typically, industrial Pt electrocatalysts are prepared by dispersing Pt powders as small as a few nanometers on conductive carbon black supports,⁴ which results in a high electrocatalytically active surface area. However, it is well-known that traditional Pt/C catalysts are easily poisoned by intermediates, most notably CO, produced during the methanol oxidation reaction at the cathode.^{5–7} In addition, these Pt/C systems suffer from poor long-term stability arising from the corrosion of the carbon support and dissolution or aggregation of Pt on the support surface.^{1,8–10} Graphene has been shown to be an excellent support for transition-metal-based electrocatalysts, impacting many of the issues above through its strong interactions with a broad range of materials,¹¹ high electronic conductivity,¹² and potential for beneficial modification of the electrochemical properties of supported clusters.¹³ However, Pt/graphene nanostructures remain poorly understood, making it challenging to optimize these electrocatalytic systems. In this article, we apply advanced

optimization methods with force fields benchmarked by first-principles theory to gain insights into Pt/graphene geometrical and electronic structures.

Several experiments have demonstrated the superior performance of Pt/graphene nanocatalysts in direct-methanol fuel cells,^{5,7,14} proton-exchange membrane fuel cells (for the oxygen reduction reaction),¹⁵ and hydrogen fuel cells.¹⁶ Such improved performance has been quantified via metrics such as electrocatalytic activity, tolerance to CO poisoning, and long-term stability toward catalyst sintering. Investigators typically attribute such improvements in catalytic performance to the synergistic interactions between the Pt catalyst and the graphene support, mediated by defects and functional groups in the graphene support that act as strong binding sites for catalyst nanoparticles.^{5,15,17–21} Computational studies corroborate this interpretation and show strong binding of Pt clusters at support defects in graphene, accompanied by a significant modification of the morphology and electronic structure of the clusters.^{9,22–30} In particular, *ab initio* studies indicate a

Received: February 5, 2016

Revised: April 23, 2016

Published: May 19, 2016



noteworthy correlation between the binding energy of a Pt cluster at support defect and the d-band center of cluster, which suggests an additional pathway for optimizing catalytic activity through defect engineering of supports.^{9,28,29} In the present work, we compare pristine and defective graphene supports to better understand how support structure alters Pt/graphene binding properties.

It is well accepted that the structure of catalyst particles plays a significant role in their catalytic performance,^{31,32} and achieving a detailed understanding of structure–activity relationships is hence an issue of much current interest. For example, in recent work Fampiou and Ramasubramaniam⁶ investigated the thermodynamic and electronic properties of Pt₁₃ isomers on graphene supports by examining both high-symmetry cluster morphologies and low-symmetry ones (derived from molecular dynamics annealing). They observed appreciable differences with respect to cluster binding energies on the support, cluster d-band centers, adsorbate binding energies, and overall charge redistribution with different cluster morphologies (isomers). While those studies were limited to a relatively small set of candidate structures, they nevertheless established the need for careful initial selection of cluster morphologies prior to subsequent studies of catalytic reactions on clusters. Indeed, for computational studies of cluster catalysis, it is reasonable to invest initial effort in ascertaining thermodynamically (or kinetically) favored structures, as these are the most probable structures under experimental conditions.³³ While ground-state cluster morphologies might, in principle, be gleaned from experiments, e.g., via fluorescence spectroscopy techniques for vacuum Pt clusters,^{34,35} such studies are extremely challenging and hence limited in number and scope. In contrast, computational studies of the energetics of Pt clusters in vacuum, using both quantum mechanics and empirical potential modeling, are more extensive.^{5,36–42} However, to the best of our knowledge, there are as yet no systematic investigations of the ground-state energetics and morphologies of Pt clusters on graphene supports. In other words, the influence of Pt–graphene binding interactions on cluster morphology and the resulting effects on cluster activity still remain to be systematically understood.

The primary goal of this paper is to present a robust methodology for identifying thermodynamically favorable structures of Pt clusters on graphene supports and to draw clear correlations between cluster energetics and catalytically relevant metrics such as the d-band center and Pt cluster charge transfer. The high-dimensional potential energy surface (PES) for the Pt/graphene system is extremely complex and a brute force search for energy minima at the first-principles level is computationally infeasible. Therefore, we carefully test and validate a Pt–C empirical potential, which we then employ within a genetic algorithm (GA)^{43–45} to facilitate rapid and thorough identification of minimum energy Pt_N (N = 2–80) clusters on defect-free and defective graphene supports. Optimized structures are then studied more thoroughly with density functional theory (DFT) calculations to test the structural accuracy and energetic ordering of the empirical potential predictions. Finally, ensembles of unsupported and supported near-minimum energy Pt₁₃ isomers are subjected to detailed electronic structure analyses via DFT calculations to identify clearly the role of support defects and cluster energetics on the potential catalytic activity of the Pt clusters. Overall, by combining an inexpensive empirical potential-based GA with *ab initio* calculations, we establish a tractable approach for

systematic exploration of supported clusters at system sizes that are experimentally relevant and yet inordinately expensive for brute force *ab initio* calculation alone.

2. COMPUTATIONAL METHODS

2.1. Genetic Algorithm for Optimization of Unsupported and Supported Clusters. Structural optimization of nanoparticles/clusters entails the nontrivial task of efficiently identifying the global minimum on a complex PES by performing unbiased sampling. Several global optimization techniques have been developed to address this challenge, including basin-hopping,^{46–50} particle-swarm optimization,^{51,52} and genetic algorithms.^{53,54} In this work, we chose to implement a genetic algorithm⁵⁵ (GA) to determine low-energy structures of unsupported and supported Pt clusters. Local energy optimization was implemented using the LAMMPS package.⁵⁶ In general, the GA produces child clusters from parent clusters by splitting parents in half and cross-mating to form children. At each new generation, local optimization is performed to drain high energies that arise from mating. Promising child clusters then become the parents for the next iteration of the GA, continued until the energies of promising clusters converge within a given tolerance. The specific approach followed here, in particular for optimization of supported clusters, follows the spirit of the pioneering work of Ho and co-workers;⁵⁷ the individual steps of the GA are discussed in detail below.

Initial Population. For a given cluster Pt_N, initial configurations for the starting generations are randomly generated with a minimum Pt–Pt distance of 1.7 Å to avoid biased searching. The distance of 1.7 Å was obtained from numerical testing; of course, no cutoff is necessary, but setting a reasonable one avoids calculating structures that will be rejected due to very short bond lengths. The quality of the *i*th cluster with energy E_i is determined by its fitness f_i , which is calculated by a linear function⁵⁵

$$f_i = 1 - 0.7\rho_i \quad (1)$$

where the scaled energy ρ_i is normalized as

$$\rho_i = (E_i - E_{\min}) / (E_{\max} - E_{\min}) \quad (2)$$

and where E_{\min} and E_{\max} are the lowest and highest energies of the initial configurations. The scaled energy ρ_i for each configuration is thus always between 0 and 1; as such, the fitness values corresponding to the lowest and highest energies are 1.0 and 0.3, respectively.

Selection. A selection operator is used to choose candidates from the current generation for mating. Here, we use the roulette wheel method of selection:⁵⁵ a configuration is chosen at random and selected for mating if its fitness value f_i is greater than a randomly generated number between 0 and 1. Otherwise, another configuration is chosen at random and tested for mating. This process is continued until two configurations are chosen for mating.

Crossover. Crossover refers to the process by which “genetic” information (coordinates) from two parent clusters is combined to generate offspring. The computational approaches for crossovers are quite different for supported and unsupported clusters. For unsupported (vacuum) clusters, the centroids of the two parent clusters are shifted to the origin, after which the parents are subjected to random rotations. The plane at $z = 0$ is used to cut each parent cluster into two parts;

the top half of parent 1 and bottom half of parent 2 are then “glued” together to form a new child. (To conserve particle number between parents and offspring, the cutting plane might require a slight offset from the $z = 0$ position.) A minimum separation of 1 Å is maintained between the glued cluster halves to avoid artificially high energies and/or forces on atoms. For supported clusters, in addition to the steps noted above, the child clusters need to be positioned appropriately relative to the graphene sheet. From numerical testing, a minimum cluster–support distance of 2 Å was found to be a good initial guess for rapid convergence.

Natural Selection. In natural evolution, individuals with higher fitness are more likely to survive and pass on their genes. In our GA, clusters with lower energies have higher fitness (eqs 1 and 2) and are chosen with higher probability for reproduction. The energy evaluation is performed using the LAMMPS package. To facilitate rapid initial relaxation of randomly generated offspring, we employ low-temperature molecular dynamics at 100 K for 0.1 ps using a 1 fs time step. Thereafter, conjugate-gradient minimization is performed for a minimum of 100 iterations or until the norm of the energy gradient on each atom is less than 10^{-3} eV/Å. The new offspring is accepted if its energy falls below an acceptance threshold

$$E_{\text{accept}} = E_{\text{min}} + N_{\text{Pt}}\Delta E \quad (3)$$

where E_{min} is the lower energy of the two parents, N_{Pt} is the number of Pt atoms in the cluster, and ΔE is a numerical parameter. The smaller the value of ΔE the more stringent is the acceptance criterion; from numerical testing, $\Delta E = 0.1$ eV was found to be a useful choice for this parameter because this value caused the algorithm to efficiently produce valid ground states. We note that this parameter (ΔE) is system-specific and can be ascertained through a small initial set of calibration runs.

Elite Species. The population size is maintained at 30 individuals throughout the optimization process. To avoid loss of high quality species, within any generation, we always maintain 20% of fittest individuals from the previous generation.

Convergence. The GA was deemed to have converged if the lowest energy clusters in each generation remained unchanged for 20 generations or if the total number of generations exceeded 1000.

2.2. Empirical Potential Models. In this work, we employ a Pt interatomic potential developed by Albe et al.⁵⁸ based on the reactive bond-order Tersoff–Brenner form.⁵⁹ In addition to Pt–Pt interactions, Albe et al.’s potential also incorporates C–C and Pt–C interactions, which makes it ideally suited for describing Pt clusters on carbon supports. In previous work, Fampiou and Ramasubramaniam⁹ showed that the potential of Albe et al. is remarkably accurate relative to DFT in describing supported cluster morphologies, albeit with limited sampling. Here, we carry out a more extensive investigation of the fidelity of this potential for unsupported clusters and show that this potential is generally in very good agreement with DFT structural models. We also perform careful tests of Albe et al.’s potential for supported clusters and demonstrate that the potential is indeed capable of delivering accurate low-energy structures for further electronic structure analyses. All empirical potential simulations are performed using the LAMMPS simulation package.

2.3. Density Functional Theory Calculations. DFT calculations are performed to study the thermodynamic and

electronic properties of selected low-energy structures using the Vienna Ab initio Simulation Package (VASP).^{60,61} Core and valence electrons are described using the projected augmented wave method.^{62,63} The Perdew–Burke–Ernzerhof (PBE)^{64–66} form of the generalized-gradient approximation is employed to describe electron exchange and correlation. A kinetic energy cutoff of 400 eV is used for the plane-wave basis set, and the conjugate gradient algorithm is used to relax ions into their ground state until the force on any atom is smaller than 0.01 eV/Å. Brillouin zone sampling is performed using a single Gamma point for unsupported clusters. For supported clusters (128 C atoms in pristine support), a $2 \times 2 \times 1$ Γ -centered k -point mesh is found to provide accuracy for energy calculations to within 0.5 meV/graphene atom. From convergence tests, at least 10 Å of vacuum is used to eliminate spurious interactions between periodic images of unsupported and/or supported clusters.

2.4. Simulation Procedure. Unsupported Pt_N ($N = 2–80$) clusters are optimized using our GA code employing Albe et al.’s empirical potential. To ensure better sampling, we run three GA simulations for each particle size, and the geometry with the lowest energy from all simulations is chosen as the global minimum. In almost all cases, the geometries obtained at the end of these three simulations are identical, indicating the robustness of GA. We also perform GA optimization of Pt_N ($N = 2–80$) clusters on defect-free (pristine) and defective (vacancy and divacancy defects) graphene supports using Albe et al.’s potential. In all supported cluster calculations, we use an 8×8 graphene supercell (128 C atoms in pristine graphene), which is sufficiently large to eliminate long-ranged interactions between Pt_{80} clusters (the largest clusters studied here). From the converged GA results, various structural properties of clusters such as the radius of gyration, coordination numbers, and average bond lengths are calculated.

By extensive exploration with the GA, we establish an ensemble of minimum and near-minimum energy Pt_N isomers; Pt_{13} isomers are chosen as a convenient example for further investigation with DFT studies. We choose five isomers of Pt_{13} clusters on pristine, vacancy, and divacancy graphene supports. These structures are subjected to additional relaxation in DFT calculations followed by electronic structure analyses.

3. RESULTS AND DISCUSSION

3.1. Structure and Energetics of Unsupported Pt Clusters. Several DFT-based studies have focused on the structure and energetics of unsupported Pt clusters,^{37,67–69} thereby providing a basis for evaluating both the quality of the empirical potential used in this work as well as the robustness of the GA. Thus, we focus first on unsupported clusters and present a critical evaluation of our simulation methods. A common shortcoming in studies of clusters is that the methods for generating low-energy structures do not use global search algorithms, relying instead on less robust techniques such as simulated annealing. Adopting high-symmetry shapes based on geometric shell models is usually incorrect for small transition-metal clusters as has been well documented in the literature.^{37,67,68} Combining global search algorithms, such as GAs, with inexpensive yet reliable empirical potentials thus offers a significant advantage for reliable and efficient sampling of the PES.

Figure 1 displays the lowest energy structures of Pt_N ($N = 2–80$) found by our GA implementation using Albe et al.’s bond-order potential. Figure 1 shows that Pt clusters are planar up to

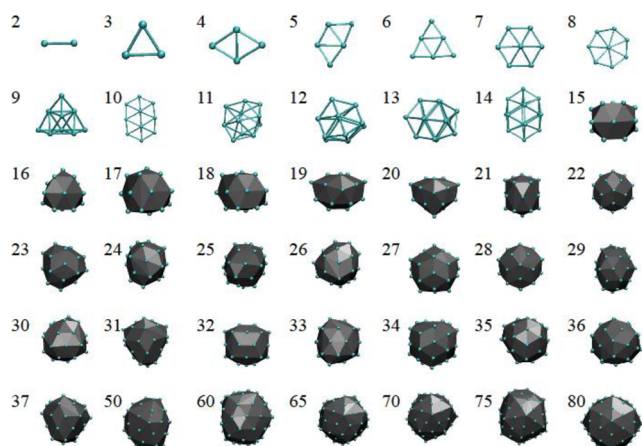


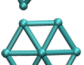


Figure 1. Minimum-energy structures of unsupported Pt clusters as predicted by our GA implementation using Albe et al.'s bond-order potential.

$N = 8$ atoms, which is consistent with the DFT study reported by Kumar et al.³⁷ Furthermore, none of the minimum-energy structures exhibit high symmetry, calling into question common assumptions about enforcing symmetry made in cluster catalysis studies. To examine the accuracy of the empirical potential in greater detail, we focus on $N = 7$ clusters as a specific example. For Pt₇ clusters, the GA predicts a centered six-member ring as the lowest energy structure (see Table 1).

Table 1. Relative Total Energies (in eV) of Pt₇ Isomers from Kumar et al.'s³⁷ and Our DFT Calculations (PBE Functional; PW91 Results in Parentheses) as Well as Albe et al.'s Empirical Potential (EP)^a

Geometry	DFT (Ref. 37)	DFT (this work)	EP
	0.00	0.00 (0.00)	unstable
	0.08	0.07 (0.06)	0.59
	0.12	0.38 (0.07)	0.00

^aEnergies are relative to the lowest energy isomer for each level of theory.

However, both Kumar et al.'s and our DFT results show that side-capped isomers turn out to be lower in energy than the centered ring. Of these side-capped structures, only one is even stable as per the empirical potential (see Table 1), and the energy is appreciably higher (~ 0.6 eV) than that of the centered-ring structure. Of course, the GA prediction can only be as good as the underlying model, and to this extent, the discrepancy between the empirical potential and DFT points to shortcomings of the former. It should be noted, though, that the centered-ring structure is fairly close in energy to the side-capped ground state at the DFT level (within 0.06–0.08 eV).

The efficacy of the combined empirical-potential and DFT approach becomes much more apparent when searching for minimum-energy structures of large clusters. As examples, we consider so-called “magic-number” Pt₁₃, Pt₅₅, Pt₁₄₇, and Pt₃₀₉ clusters, which have been studied widely in their high-symmetry cuboctahedral (O_h) and icosahedral (I_h) structural motifs.^{40,70,71}

As before, we use the GA to find minimum-energy structures for these various cluster sizes and then further relax the minimum-energy structures in DFT (Figure 2). The energies of

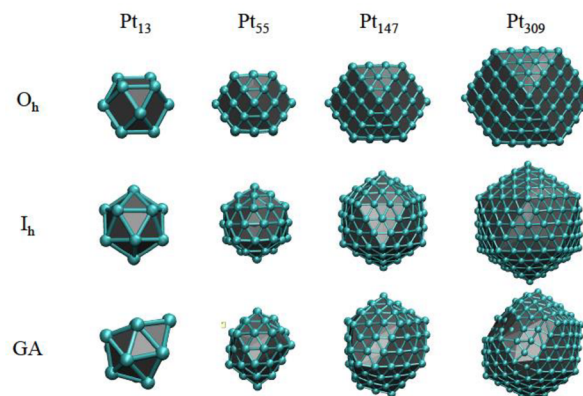


Figure 2. Geometries of low-energy “magic-number” Pt isomers in vacuum. The first two rows display high symmetry cuboctahedral (O_h) and icosahedral (I_h) clusters. The third row displays minimum-energy structures found by the genetic algorithm with an empirical potential.

the DFT-relaxed structures are then compared with corresponding DFT energies for the high-symmetry O_h and I_h structures; total energy differences relative to the minimum-energy structure for each cluster size are reported in Table 2.

Table 2. Relative Total Energies (in eV) of High-Symmetry (Cuboctahedral: O_h ; Icosahedral: I_h) Pt Clusters and GA-Optimized, Low-Energy Clusters Calculated Using DFT and Albe et al.'s Empirical Potential (EP)^a

	Pt ₁₃		Pt ₅₅		Pt ₁₄₇		Pt ₃₀₉	
	DFT	EP	DFT	EP	DFT	EP	DFT	EP
I_h	1.3	1.7	3.3	3.4	6.5	5.1	7.7	5.6
O_h	2.0	1.8	5.1	6.4	8.2	12.4	9.7	18.4
GA	0.0	0.0	0.0	0.0	0.0	0.0	0.0	0.0

^aEnergies are relative to the lowest energy isomer for each size and level of theory.

These results show clearly that the high-symmetry structures are not the lowest-energy structures, as was also shown in previous DFT studies of Pt₁₃ and Pt₅₅ clusters.^{40,69} Indeed, the results obtained here for larger clusters are particularly striking and prompt interesting questions regarding typical sizes at which transitions from low-symmetry to high-symmetry clusters may be expected to occur in faceted crystals of Pt nanoclusters; such issues will be discussed elsewhere.

It is also apparent from these results that the performance of Albe et al.'s empirical potential—in terms of relative energetic ordering of structures—is surprisingly good when compared with DFT calculations, especially considering that the potential was parametrized for bulk properties. The lowest-energy structures found by the GA essentially resemble defective icosahedra that are approximately 0.01–0.1 eV/atom lower in energy (across the entire range of sizes) than the perfect icosahedra. Cuboctahedral structures are in general higher in energy than both the GA-optimized structures and the perfect icosahedra.

Overall, the benchmarking studies presented here lead us to two principal conclusions. First, Albe et al.'s bond-order

potential is of sufficient accuracy to deliver near-minimum energy structures of unsupported clusters, which can then be subjected to additional optimization in DFT calculations. Second, our GA implementation is able to deliver reliable minimum-energy results for unsupported clusters, which then lends us confidence in proceeding to the study of supported clusters, the primary target of this work and the subject of the next discussion.

3.2. Structure and Energetics of Graphene-Supported Pt Clusters. We now consider the energetics of Pt_N clusters on graphene supports. As model supports, we use graphene sheets that are either defect-free (pristine) or sheets that contain point defects (vacancies and divacancies). Point defects in graphene are known to act as strong anchoring sites for nanoclusters and have also been shown to modify the electronic structure and catalytic activity of small clusters.^{9,28,29} The metrics we adopt for thermodynamic comparisons are the cluster adsorption energy and the overall formation energy of the composite Pt/graphene system. The adsorption energy (E_{ad}) is defined as

$$E_{ad} = E_{Pt_N+Gr} - E_{Pt_N} - E_{Gr} \quad (4)$$

where E_{Pt_N+Gr} is the total energy of the Pt/graphene system, E_{Pt_N} is the total energy of the Pt_N cluster without the support, and E_{Gr} is the total energy of the (pristine/defective) graphene sheet. The overall formation energy of the composite Pt/graphene system (E_f) is defined as

$$E_f = E_{Pt_N+Gr} - ME_C - NE_{Pt} \quad (5)$$

where E_{Pt_N+Gr} is the total energy of the Pt/graphene system, E_{Pt} is the energy of an isolated Pt atom in vacuum, E_C is the energy of a single C atom in graphene, and M and N are the number of C and Pt atoms, respectively.

First, to test the performance of our GA, we study supported Pt_N ($N = 2, 3, 4, 13$) clusters and compare our results with those of Fampiou and Ramasubramanian,⁹ who also used Albe et al.'s bond-order potential but adopted a molecular dynamics (MD) annealing scheme for energy minimization. The formation energies for Pt_N ($N = 2, 3, 4, 13$) clusters with pristine and defective graphene supports are reported in Table 3, and the corresponding structures (from the GA) are

Table 3. Formation Energies (eV) of Minimum-Energy Pt Clusters on Pristine and Defective (Vacancy, Divacancy) Graphene Supports Identified Using the GA and by Molecular-Dynamics-Based Annealing (Ref 9)

	pristine		vacancy		divacancy	
	GA	annealing	GA	annealing	GA	annealing
Pt ₂	-5.75	-5.62	-5.33	-5.30	-5.59	-5.25
Pt ₃	-10.11	-10.06	-9.55	-8.73	-9.88	-8.38
Pt ₄	-14.24	-13.12	-13.80	-11.69	-14.13	-13.80
Pt ₁₃	-55.50	-55.20	-55.16	-55.14	-55.65	-55.67

displayed in Figure 3. For additional comparison, we also report formation energies calculated using the empirical potential in the Supporting Information (Table S1). In all cases, the GA delivers structures with lower formation energies than the MD annealing results previously reported. The differences are particularly noticeable for few-atom clusters. In the Pt₂ case, the GA produces ground states consisting of dimer orientations parallel to the surface on pristine and defective graphene supports. MD-based annealing consistently generates

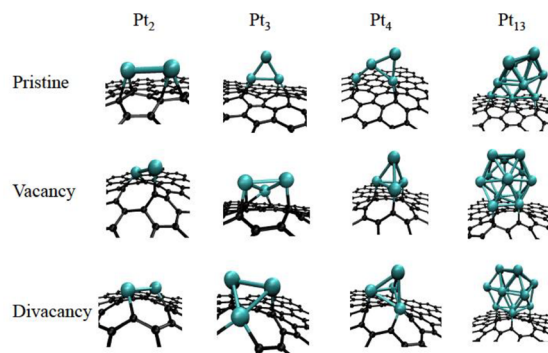


Figure 3. Minimum-energy structures of Pt_N ($N = 2, 3, 4, 13$) on pristine graphene (upper row) and graphene with single vacancy (middle row) and divacancy defects (bottom row).

local minima with vertically oriented Pt dimers on pristine graphene; on defective graphene, the dimers lie parallel to the support. For Pt₃ clusters on pristine graphene, both GA and MD annealing find the vertical triangle as the ground state; on defective graphene, the GA finds structures that are appreciably more stable by 1.0–1.5 eV than those from MD annealing. For Pt₄ clusters, the GA finds a planar cluster that is nearly vertically oriented to the pristine graphene sheet as the minimum-energy structure; a tetrahedron is the most stable structure on defective graphene supports. The MD annealing algorithm is again stuck in various local minima at higher energies. Finally, for Pt₁₃ clusters on graphene supports, Fampiou and Ramasubramanian showed that the clusters prefer more open structures instead of high-symmetry ones (I_h or O_h); the GA results confirm those findings, and the minimum-energy structures are also energetically very close to those found by MD annealing. It thus appears that clusters with very small number of atoms present pathological challenges for the MD annealing procedure, in particular, capturing the precise orientation and location of cluster atoms on the support. With increasing cluster sizes, the energetics appear to be dominated by the inherent morphology of the cluster itself, with orientational effects relative to the support being of lesser importance. In any case, it is clear that a global minimization algorithm, such as a GA, performs more reliably at finding ground states than *ad hoc* procedures such as simulated annealing.

Next, we study the properties of supported Pt_N clusters over the size range $N = 2–80$ analogous to the unsupported cluster studies. In addition to thermodynamic properties such as adsorption and formation energies, we also thoroughly characterize the structural properties of clusters through metrics such as the radius of gyration, average coordination number, average bond lengths, and fraction of (potentially) catalytically active surface atoms, which are variously displayed in Figure 4. Note that while the catalytic activity of a site on a crystalline facet (terrace, step, edge, kink) or on a large nanoparticle (face, edge, corner) can vary significantly due to local coordination, the nanoclusters considered here are too small to display such distinguishing morphological features. Thus, we focus on understanding average properties of surface sites throughout this work. The various configurations studied here are all minimum-energy structures obtained via the GA.

Figure 4a displays the radius of gyration (R_g) of Pt_N clusters with and without the graphene support. As seen, R_g tends to be noticeably higher for unsupported clusters and clusters on pristine graphene supports relative to those on defective

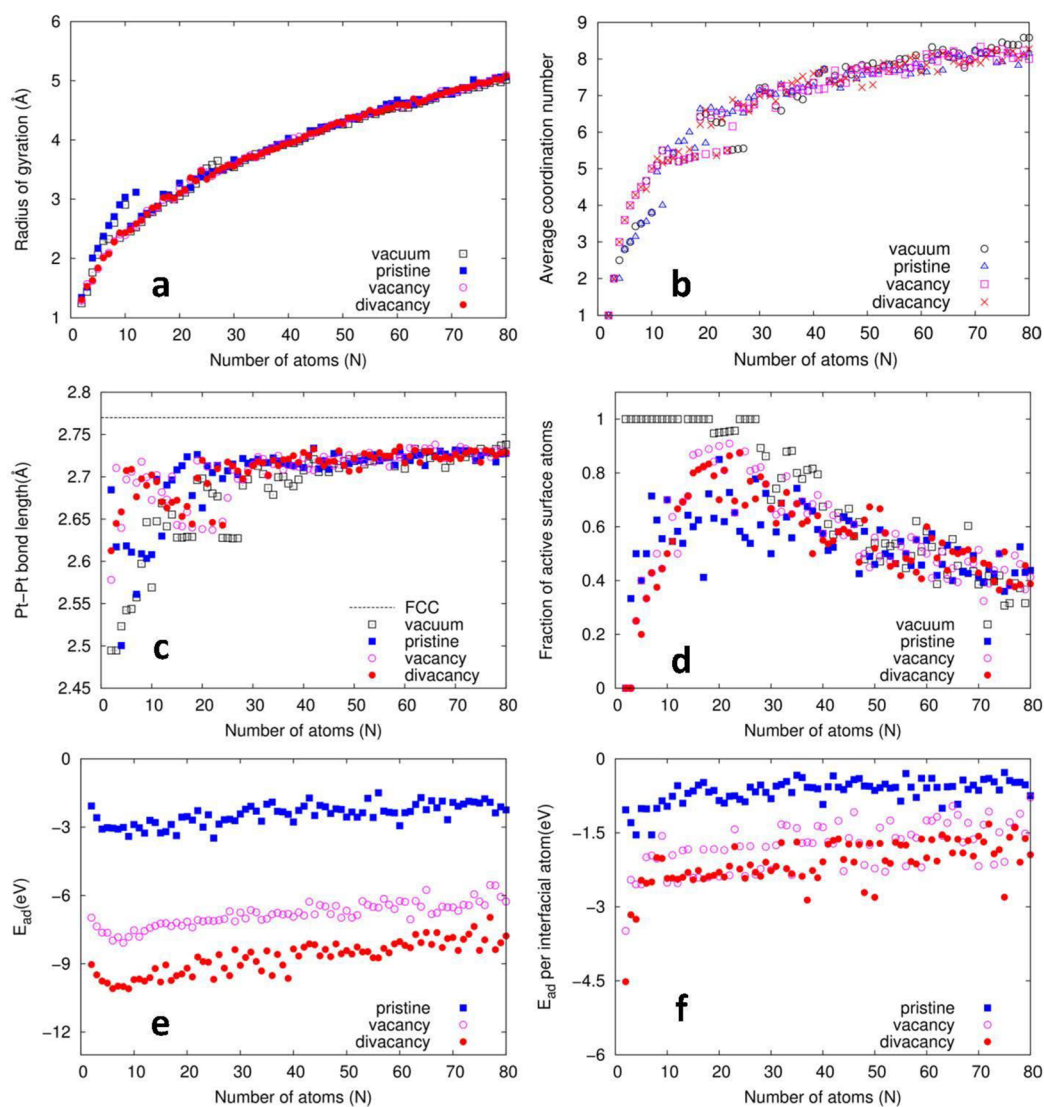


Figure 4. Evolution of structural and energetic properties of global minima of Pt_N/graphene calculated using the genetic algorithm as a function of particle number N : (a) radius of gyration; (b) average coordination number of Pt atoms (excluding Pt–C bonds); (c) average Pt–Pt bond length (dashed line is for bulk FCC Pt); (d) fraction of active surface atoms, defined in eq 6; (e) adsorption energy (E_{ad}) of Pt clusters on graphene; (f) average contribution of Pt atoms at the Pt–C interface to E_{ad} .

supports up to $N = 12$. This is due to 2D morphologies being preferable both in vacuum and on pristine graphene supports at these cluster sizes; the presence of point defects in the graphene support favors 3D structures beginning from the smallest possible size, Pt₄, as seen in Figure 3. For $N \geq 13$, the support effect on cluster morphology is negligible— R_g is approximately the same for supported as well as unsupported clusters. Physically, this result suggests that the Pt–C contribution to the total energy becomes less important compared with the Pt–Pt interaction for larger clusters.

Another important structural metric used to characterize clusters is the atomic coordination number; Figure 4b displays the average coordination number (Z_{avg}) of Pt atoms as a function of cluster size. The precise number of neighbors of an atom is sensitive to the cutoff distance chosen for bond counting, and for consistency, we use the same cutoff distance as that for Pt–Pt interactions in the bond-order potential (3.3 Å). As seen from Figure 4b, the average coordination number increases monotonically with cluster size, as is to be expected due to the increase in the bulk-to-surface ratio. For the range of

clusters studied here, $Z_{avg} = 8$ is the largest value attained; for reference, we recall that the coordination number of atoms on the Pt(111) surface is 9 while that in the bulk is 12. This significant overall degree of undercoordination is to be expected for such small clusters that are mostly “surface” rather than “bulk”. Our calculations show that the smallest cluster size for which at least one atom has a coordination number of 12 is $N = 19$.

Figure 4c offers insight complementary to this analysis of coordination numbers by displaying the average Pt–Pt bond length (a_{avg}) in the unsupported and supported Pt clusters; the horizontal dashed line in that figure indicates the bulk, FCC Pt–Pt bond length (2.77 Å) for comparison. The average Pt–Pt bond decreases in length with decreasing cluster size, which once again reflects the increase in the ratio of surface to bulk atoms as undercoordinated surface atoms exhibit shorter bonds to compensate for having fewer neighbors. The trends for a_{avg} are similar for unsupported clusters and for those on pristine graphene supports, especially at small cluster sizes, reflecting the relatively small role of the support in the absence of strong

perturbations such as those arising from point defects. Again, for larger clusters, the differences in a_{avg} are small, thus reflecting the relatively minor role of the support on cluster morphology. For the range of cluster sizes studied here, a_{avg} is still about 0.1 Å smaller than the bulk FCC value. There are some systematic deviations in the monotonic growth of Z_{avg} and a_{avg} in the $N = 20$ –40 as seen from Figures 4b and 4c. Closer visual inspection of these clusters leads us to attribute the fluctuations to a competition between hollow-core and filled-center cluster morphologies.

A structural property of interest and immediate relevance to cluster catalysis is the number of potentially active Pt atoms on the cluster surface. Atoms within the interior of the cluster do not directly participate in surface reactions, and we also assume that atoms directly bonded to the support are less likely to participate in surface reactions due to constraints arising from e.g. steric hindrance and possibly from electronic effects (saturation of dangling bonds). There are of course exceptions to such criteria, notably for single-site catalysts bound at point defects in graphene,^{72,73} but these are essentially pathological cases and the proposed criterion is both intuitively appealing and physically reasonable for larger clusters. Thus, we define the fraction of active surface atoms ($f_{\text{Pt}}^{\text{surf}}$) as

$$f_{\text{Pt}}^{\text{surf}} = (N_{\text{Pt}}^{\text{surf}} - N_{\text{Pt}}^{\text{C}})/N_{\text{Pt}} \quad (6)$$

where $N_{\text{Pt}}^{\text{surf}}$ is the number of atoms on the surface of the Pt cluster and N_{Pt}^{C} is the number of Pt atoms bonded to the support. Various criteria may be established for identifying a “surface” atom; we do so here by assigning an atom with six or fewer neighbors to be a surface atom. Visual inspection of several clusters confirms the validity of this coordination number cutoff. As seen from Figure 4d, $f_{\text{Pt}}^{\text{surf}}$ displays rather interesting behavior. For unsupported clusters all atoms are on the surface for $N < 19$; for larger unsupported clusters, most of the Pt atoms are in the bulk and consequently are not active. For supported clusters, the fraction of active sites is initially small as many Pt atoms are bonded directly to the graphene support; at large cluster sizes, most of the Pt atoms are again in the bulk and are consequently not active. The optimal value for $f_{\text{Pt}}^{\text{surf}}$ is achieved in the range $N = 20$ –30 irrespective of the presence or absence of the support defects. This is a key result as it identifies an optimal range of cluster sizes that maximally utilizes the precious metal catalyst; to the best of our knowledge, this result has not been reported before and, in particular, not for supported Pt clusters.

Finally, Figures 4e and 4f display the total adsorption energy and adsorption energy per interfacial Pt atom for supported Pt_N clusters. It is clear that point defects in the graphene support bind Pt clusters more strongly than does pristine graphene across the entire range of cluster sizes; divacancies are also seen to be stronger binding sites than vacancies due to a higher number of dangling bonds. In general, the variation in adsorption energies with cluster size is rather small; similar results were reported by Ramos-Sanchez et al.,⁷⁴ who used DFT calculations to study clusters on graphite in the range of $N = 1$ –38. The slight decrease in binding strength (less negative adsorption energies) with increasing cluster sizes (beyond $N = 10$) is indicative of weaker trapping of larger clusters by the vacancy/divacancy, thus suggesting the need for larger support defects to improve the stability of larger Pt clusters against aggregation.

3.3. Electronic Structure of Pt_{13} Isomers. It is well-known that chemisorption of adsorbates on transition metal surfaces is strongly correlated with the so-called d-band center energy of the surface.⁷⁵ Several studies have now extended this metric to the study of supported clusters and shown similar correlations.^{27,29,76} In particular, the influence of cluster morphology as well as the role of the support in modulating the d-band center energy are issues of current interest for rational catalyst design. Our ability to produce low-energy isomers at low computational expense using the GA now allows us to examine more broadly the issues of cluster morphology and support effects on the catalytic activity of clusters (beyond the limited cases studied in our previous work^{9,29}). As an example, we focus here on Pt_{13} clusters; more comprehensive studies across a range of cluster sizes will be reported elsewhere.

Using the GA, we identified several Pt_{13} isomers within a 30 meV/atom energy window close to the global minimum for Pt_{13} in vacuum or with various support types. All candidates, supported or otherwise, were imported into VASP and subjected to conjugate-gradient structural relaxation. For vacuum Pt_{13} isomers, an additional 15 candidates were obtained by simply eliminating the support from the low-energy Pt_{13} /graphene systems and relaxing the residual Pt_{13} cluster; such clusters are merely local rather than global minima, but including these in our analyses gives us a larger statistical sample for studying structure–property correlations. From the angular-momentum-projected density of states, we compute the d-band center energy (ϵ_{d}) as

$$\epsilon_{\text{d}} = \frac{\int \rho E \, dE}{\int \rho \, dE} \quad (7)$$

where E is energy of each state and ρ is the corresponding density of d-states. Figure 5a displays d-band center energies as a function of cluster adsorption energy and formation energy for supported and unsupported clusters, respectively. For unsupported clusters, the d-band center energy varies almost linearly with the formation energy and spans about 0.1 eV within a formation energy window of width 0.2 eV/atom. In the presence of the graphene support, ϵ_{d} can be significantly lowered, especially in the presence of vacancy and divacancy defects, and once again the lowering of the d-band center is correlated with the adsorption energy, which was also noted earlier by Fampiou and Ramasubramaniam.⁹ In general, for the various clusters on defective supports, we find that when a Pt atom occupies the center of the defect (vacancy/divacancy), the total energy as well as the adsorption energy decrease significantly, as indicated by the points within the dashed square in Figure 5a; this decrease in adsorption energy is accompanied by a drop in the d-band center energy. Furthermore, for all cases of clusters on defective supports, the d-band center lies slightly below that for Pt(111), suggesting comparable or possibly weaker adsorbate binding. In the absence of point defects, the cluster d-band center approximately coincides with the calculated value for Pt(111); for unsupported clusters, the d-band centers are appreciably higher than that for Pt(111).

As noted in prior work,^{9,27} the total charge transferred from the cluster to graphene is an important factor in shifting the cluster d-band center. Thus, we also perform a Bader charge analysis^{77,78} to evaluate the total charge transferred from the cluster to the graphene support. Figure 5b displays the transferred charge with respect to the adsorption energy, and

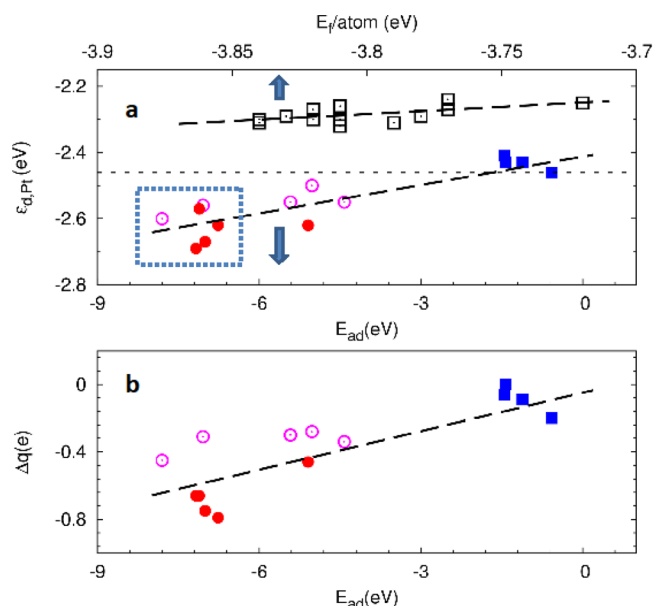


Figure 5. Position of d-band center ($\epsilon_{d,Pt}$) relative to the Fermi level (a) and net charge transferred (b) to Pt₁₃ isomers in vacuum and on graphene support. Data for Pt₁₃ clusters in vacuum and on support are plotted with respect to the formation energy (E_i) per atom and the adsorption energy (E_{ad}), respectively. The horizontal dashed line represents $\epsilon_{d,Pt}$ for the Pt(111) surface. Other dashed lines are guides to the eyes. Points inside dashed square correspond to structures with Pt atoms occupying the center of the defect.

the trends are similar to that of the d-band analysis. Similar to previous reports,⁹ we observe that stronger binding of clusters to the support results in greater depletion of charge from the cluster, which then leads to a lowering of the d-band center of the cluster. A complementary and chemically intuitive view of bonding at the Pt–C interface can also be obtained from a natural bond orbital (NBO) analysis,^{79,80} which we present in the Supporting Information. Broadly speaking, the NBO analysis does not show any significant bonding between Pt₁₃ clusters and pristine graphene; for the defective graphene supports, a predominantly covalent nature is found for C–Pt bonds at the defect center with clear polarization toward the C atoms, which bolsters the picture of charge transfer from Pt to graphene obtained from the Bader analysis.

The electronic structure analysis presented here is essentially in agreement with previous work by Fampiou and Ramasubramanian,⁹ among others,²⁷ although with much better statistics and more careful attention to computational procedures for generating low-energy structures. The role of the support is relatively clear in our studies: defective supports appreciably lower the d-band centers, at least of small Pt clusters, and consequently have implications for adsorbate binding and reaction barriers.^{28,29} In terms of proper selection of structures for electronic structure analyses and/or studies of reaction pathways, it would appear that small deviations from the minimum-energy cluster morphology are unlikely to lead to large deviations in the energies of the surface states at least for small clusters. Thus, we expect that any reasonably robust method for generating low-energy morphologies ought to result in plausible predictions of catalytic behavior from subsequent electronic structure studies.

Finally, data for adsorption energies of several clusters of varying sizes on defective and defect-free graphene supports are

displayed in the Supporting Information (Figure S1), as are the charge transfer data associated with these various cases (Figure S2). As shown there, the adsorption energy of Pt_N clusters to the graphene supports increases weakly (i.e., binding becomes less strong) with increasing cluster size. Associated with this inverse correlation between adsorption energy and cluster size, we also see that the extent of charge transfer is also reduced at larger cluster sizes. Additional electronic structure analyses to investigate these results with more extensive statistical sampling are underway and will be reported elsewhere.

4. CONCLUSIONS

We have implemented an empirical-potential-based genetic algorithm for structural optimization of unsupported and supported Pt nanoclusters. Using a bond-order potential for the Pt–C system developed by Albe et al., we explored the morphological properties of Pt_N ($N = 2–80$) clusters considering unsupported clusters as well as those supported on pristine or defective graphene supports. A key finding from the structural analysis is that the fraction of potentially active surface sites for supported Pt clusters is maximal for 20–30 atom clusters irrespective of the presence or absence of support defects; this result provides a useful synthetic target for optimal utilization of the precious metal catalyst. Selected ground-state clusters from the GA process were subjected to structural relaxation with DFT calculations and compared with corresponding high-symmetry icosahedral and cuboctahedral clusters. For all “magic number” clusters, the GA optimization process produced cluster morphologies that are lower in energy than their high-symmetry counterparts (at both the empirical potential and DFT levels). The inclusion of the graphene support is found to influence cluster morphologies at very small sizes; beyond ~ 10 atoms, the cluster morphology is essentially dominated by Pt–Pt interactions with minimal perturbations from the support, at least for the cases considered here with small point defects in the support. The effect of the support—more precisely support defects—on the electronic properties of Pt clusters is more pronounced. For the cases of supported Pt₁₃ clusters studied here, the cluster d-band energy is downshifted relative to the Fermi level in direct proportion to the strength of binding of the cluster to the support. Cluster adsorption energies on the support and the attendant d-band shifts are sensitive to the precise details of bonding at the cluster–support interface, especially for small clusters, requiring careful structural optimization.

By integrating computationally inexpensive empirical-potential-based GAs for global structural optimization with DFT modeling for local minimization and electronic structure analyses, we have demonstrated a viable approach for systematic studies of supported catalyst nanoclusters. While this work was restricted to the Pt–C system, there is no fundamental impediment to applying similar approaches to multicomponent catalyst clusters on various supports as long as appropriate interatomic potentials, preferably of low computational complexity, are available for the systems of interest. Advances along such directions for supported alloy nanoclusters will be reported in future work.

■ ASSOCIATED CONTENT

Supporting Information

The Supporting Information is available free of charge on the ACS Publications website at DOI: 10.1021/acs.jpcc.6b01288.

DFT calculations of adsorption energies of Pt_N (N = 20–80) clusters on graphene; comparison of DFT vs bond-order potential formation energies of Pt–graphene composite systems; natural bond orbital analysis of Pt₁₃ clusters adsorbed at vacancy and divacancy defects in graphene (PDF)

AUTHOR INFORMATION

Corresponding Authors

*E-mail: auerbach@chem.umass.edu (S.M.A.).

*E-mail: ashwin@engin.umass.edu (A.R.).

Notes

The authors declare no competing financial interest.

ACKNOWLEDGMENTS

H.S. and A.R. gratefully acknowledge research funding from the U.S. Department of Energy under Award DE-SC0010610. Computational resources were provided by the Massachusetts Green High Performance Computing Center and also by the National Energy Research Scientific Computing Center, which is supported by the Office of Science of the U.S. Department of Energy under Contract DE-AC02-05CH11231.

REFERENCES

- (1) Yu, X. W.; Ye, S. Y. Recent advances in activity and durability enhancement of Pt/C catalytic cathode in PEMFC - Part I. Physico-chemical and electronic interaction between Pt and carbon support, and activity enhancement of Pt/C catalyst. *J. Power Sources* **2007**, *172*, 133–144.
- (2) Zhang, S. S.; Yuan, X. Z.; Hin, J. N. C.; Wang, H. J.; Friedrich, K. A.; Schulze, M. A review of platinum-based catalyst layer degradation in proton exchange membrane fuel cells. *J. Power Sources* **2009**, *194*, 588–600.
- (3) Antolini, E.; Salgado, J. R. C.; Gonzalez, E. R. The stability of Pt-M (M = first row transition metal) alloy catalysts and its effect on the activity in low temperature fuel cells - A literature review and tests on a Pt-Co catalyst. *J. Power Sources* **2006**, *160*, 957–968.
- (4) Song, W. Y.; Chen, Z. X.; Yang, C.; Yang, Z. P.; Tai, J. P.; Nan, Y. L.; Lu, H. B. Carbon-coated, methanol-tolerant platinum/graphene catalysts for oxygen reduction reaction with excellent long-term performance. *J. Mater. Chem. A* **2015**, *3*, 1049–1057.
- (5) Li, Y. J.; Gao, W.; Ci, L. J.; Wang, C. M.; Ajayan, P. M. Catalytic performance of Pt nanoparticles on reduced graphene oxide for methanol electro-oxidation. *Carbon* **2010**, *48*, 1124–1130.
- (6) Wen, Z. H.; Liu, J.; Li, J. H. Core/shell Pt/C nanoparticles embedded in mesoporous carbon as a methanol-tolerant cathode catalyst in direct methanol fuel cells. *Adv. Mater.* **2008**, *20*, 743–747.
- (7) Yoo, E.; Okata, T.; Akita, T.; Kohyama, M.; Nakamura, J.; Honma, I. Enhanced Electrocatalytic Activity of Pt Subnanoclusters on Graphene Nanosheet Surface. *Nano Lett.* **2009**, *9*, 2255–2259.
- (8) Shao, Y. Y.; Wang, J.; Kou, R.; Engelhard, M.; Liu, J.; Wang, Y.; Lin, Y. H. The corrosion of PEM fuel cell catalyst supports and its implications for developing durable catalysts. *Electrochim. Acta* **2009**, *54*, 3109–3114.
- (9) Fampiou, I.; Ramasubramaniam, A. Binding of Pt Nanoclusters to Point Defects in Graphene: Adsorption, Morphology, and Electronic Structure. *J. Phys. Chem. C* **2012**, *116*, 6543–6555.
- (10) Yu, X. W.; Ye, S. Y. Recent advances in activity and durability enhancement of Pt/C catalytic cathode in PEMFC - Part II: Degradation mechanism and durability enhancement of carbon supported platinum catalyst. *J. Power Sources* **2007**, *172*, 145–154.
- (11) Park, S.; Ruoff, R. S. Chemical methods for the production of graphenes. *Nat. Nanotechnol.* **2009**, *4*, 217–224.
- (12) Yang, J.; Zang, C. L.; Sun, L.; Zhao, N.; Cheng, X. N. Synthesis of graphene/Ag nanocomposite with good dispersibility and electro-

conductivity via solvothermal method. *Mater. Chem. Phys.* **2011**, *129*, 270–274.

- (13) Wang, C. M.; Ma, L.; Liao, L. W.; Bai, S.; Long, R.; Zuo, M.; Xiong, Y. J. A unique platinum-graphene hybrid structure for high activity and durability in oxygen reduction reaction. *Sci. Rep.* **2013**, *3*, 2580.

- (14) Huang, H. J.; Chen, H. Q.; Sun, D. P.; Wang, X. Graphene nanoplate-Pt composite as a high performance electrocatalyst for direct methanol fuel cells. *J. Power Sources* **2012**, *204*, 46–52.

- (15) Kou, R.; et al. Enhanced activity and stability of Pt catalysts on functionalized graphene sheets for electrocatalytic oxygen reduction. *Electrochem. Commun.* **2009**, *11*, 954–957.

- (16) Seger, B.; Kamat, P. V. Electrocatalytically Active Graphene-Platinum Nanocomposites. Role of 2-D Carbon Support in PEM Fuel Cells. *J. Phys. Chem. C* **2009**, *113*, 7990–7995.

- (17) Tang, Y. N.; Yang, Z. X.; Dai, X. Q. Trapping of metal atoms in the defects on graphene. *J. Chem. Phys.* **2011**, *135*, 224704.

- (18) Rodriguez-Manzo, J. A.; Cretu, O.; Banhart, F. Trapping of Metal Atoms in Vacancies of Carbon Nanotubes and Graphene. *ACS Nano* **2010**, *4*, 3422–3428.

- (19) Gan, Y. J.; Sun, L. T.; Banhart, F. One- and two-dimensional diffusion of metal atoms in graphene. *Small* **2008**, *4*, 587–591.

- (20) Wu, G. H.; Huang, H.; Chen, X. M.; Cai, Z. X.; Jiang, Y. Q.; Chen, X. Facile synthesis of clean Pt nanoparticles supported on reduced graphene oxide composites: Their growth mechanism and tuning of their methanol electro-catalytic oxidation property. *Electrochim. Acta* **2013**, *111*, 779–783.

- (21) He, D. P.; Cheng, K.; Li, H. G.; Peng, T.; Xu, F.; Mu, S. C.; Pan, M. Highly Active Platinum Nanoparticles on Graphene Nanosheets with a Significant Improvement in Stability and CO Tolerance. *Langmuir* **2012**, *28*, 3979–3986.

- (22) Tang, Y. A.; Yang, Z. X.; Dai, X. Q. A theoretical simulation on the catalytic oxidation of CO on Pt/graphene. *Phys. Chem. Chem. Phys.* **2012**, *14*, 16566–16572.

- (23) Durbin, D. J. D.; Malarier-Jugroot, C. Density Functional Theory Analysis of Metal/Graphene Systems As a Filter Membrane to Prevent CO Poisoning in Hydrogen Fuel Cells. *J. Phys. Chem. C* **2011**, *115*, 808–815.

- (24) Zhou, M.; Zhang, A. H.; Dai, Z. X.; Zhang, C.; Feng, Y. P. Greatly enhanced adsorption and catalytic activity of Au and Pt clusters on defective graphene. *J. Chem. Phys.* **2010**, *132*, 194704.

- (25) Kim, G.; Jhi, S. H. Carbon Monoxide-Tolerant Platinum Nanoparticle Catalysts on Defect-Engineered Graphene. *ACS Nano* **2011**, *5*, 805–810.

- (26) Lim, D. H.; Wilcox, J. Mechanisms of the Oxygen Reduction Reaction on Defective Graphene-Supported Pt Nanoparticles from First-Principles. *J. Phys. Chem. C* **2012**, *116*, 3653–3660.

- (27) Lim, D. H.; Wilcox, J. DFT-Based Study on Oxygen Adsorption on Defective Graphene-Supported Pt Nanoparticles. *J. Phys. Chem. C* **2011**, *115*, 22742–22747.

- (28) Fampiou, I.; Ramasubramaniam, A. Influence of Support Effects on CO Oxidation Kinetics on CO-Saturated Graphene-Supported Pt-13 Nanoclusters. *J. Phys. Chem. C* **2015**, *119*, 8703–8710.

- (29) Fampiou, I.; Ramasubramaniam, A. CO Adsorption on Defective Graphene-Supported Pt-13 Nanoclusters. *J. Phys. Chem. C* **2013**, *117*, 19927–19933.

- (30) Okamoto, Y. Density-functional calculations of icosahedral M-13 (M = Pt and Au) clusters on graphene sheets and flakes. *Chem. Phys. Lett.* **2006**, *420*, 382–386.

- (31) Zhang, L.; Anderson, R. M.; Crooks, R. M.; Henkelman, G. Correlating Structure and Function of Metal Nanoparticles for Catalysis. *Surf. Sci.* **2015**, *640*, 65–72.

- (32) Smith, G. V.; Tjandra, S.; Musoiu, M.; Wiltowski, T.; Notheisz, F.; Bartok, M.; Hannus, I.; Ostgard, D.; Malhotra, V. Modified activities and selectivities of silated-oxidized-reduced Pd and Pt catalysts. *J. Catal.* **1996**, *161*, 441–450.

- (33) Hartke, B. Global cluster geometry optimization by a phenotype algorithm with niches: Location of elusive minima, and low-order scaling with cluster size. *J. Comput. Chem.* **1999**, *20*, 1752–1759.

- (34) Airola, M. B.; Morse, M. D. Rotationally resolved spectroscopy of Pt-2. *J. Chem. Phys.* **2002**, *116*, 1313–1317.
- (35) Fabbri, J. C.; Langenberg, J. D.; Costello, Q. D.; Morse, M. D.; Karlsson, L. Dispersed fluorescence spectroscopy of jet-cooled AgAu and Pt-2. *J. Chem. Phys.* **2001**, *115*, 7543–7549.
- (36) Wang, X. L.; Tian, D. X. Structures and structural evolution of Pt-*n* (*n* = 15–24) clusters with combined density functional and genetic algorithm methods. *Comput. Mater. Sci.* **2009**, *46*, 239–244.
- (37) Kumar, V.; Kawazoe, Y. Evolution of atomic and electronic structure of Pt clusters: Planar, layered, pyramidal, cage, cubic, and octahedral growth. *Phys. Rev. B: Condens. Matter Mater. Phys.* **2008**, *77*, 205418.
- (38) Sebetci, A.; Guvenc, Z. B. Global minima of Al(*N*), Au(*N*) and Pt(*N*), *N* ≤ 80, clusters described by the Voter-Chen version of embedded-atom potentials. *Modell. Simul. Mater. Sci. Eng.* **2005**, *13*, 683–698.
- (39) Sebetci, A.; Guvenc, Z. B. Global minima for free Pt-*N* clusters (*N* = 22–56): a comparison between the searches with a molecular dynamics approach and a basin-hopping algorithm. *Eur. Phys. J. D* **2004**, *30*, 71–79.
- (40) Xiao, L.; Wang, L. C. Structures of platinum clusters: Planar or spherical? *J. Phys. Chem. A* **2004**, *108*, 8605–8614.
- (41) Sebetci, A.; Guvenc, Z. B. Energetics and structures of small clusters: Pt(*N*), *N* = 2–21. *Surf. Sci.* **2003**, *525*, 66–84.
- (42) Tian, W. Q.; Ge, M. F.; Sahu, B. R.; Wang, D. X.; Yamada, T.; Mashiko, S. Geometrical and electronic structure of the Pt-7 cluster: A density functional study. *J. Phys. Chem. A* **2004**, *108*, 3806–3812.
- (43) Pittaway, F.; Paz-Borbon, L. O.; Johnston, R. L.; Arslan, H.; Ferrando, R.; Mottet, C.; Barcaro, G.; Fortunelli, A. Theoretical Studies of Palladium-Gold Nanoclusters: Pd-Au Clusters with up to 50 Atoms. *J. Phys. Chem. C* **2009**, *113*, 9141–9152.
- (44) Borbon-Gonzalez, D. J.; Pacheco-Contreras, R.; Posada-Amarillas, A.; Schon, J. C.; Johnston, R. L.; Montejano-Carrizales, J. M. Structural Insights into 19-Atom Pd/Pt Nanoparticles: A Computational Perspective. *J. Phys. Chem. C* **2009**, *113*, 15904–15908.
- (45) Chen, F. Y.; Johnston, R. L. Structure and spectral characteristics of the nanoalloy Ag₃Au₁₀. *Appl. Phys. Lett.* **2007**, *90*, 153123.
- (46) Priest, C.; Tang, Q.; Jiang, D. E. Structural Evolution of Tc-*n* (*n* = 4–20) Clusters from First-Principles Global Minimization. *J. Phys. Chem. A* **2015**, *119*, 8892–8897.
- (47) Arslan, H. Structures and energetic of Palladium-Cobalt binary clusters. *Int. J. Mod. Phys. C* **2008**, *19*, 1243–1255.
- (48) Gould, A. L.; Heard, C. J.; Logsdail, A. J.; Catlow, C. R. A. Segregation effects on the properties of (AuAg)₍₁₄₇₎. *Phys. Chem. Chem. Phys.* **2014**, *16*, 21049–21061.
- (49) Ouyang, R. H.; Xie, Y.; Jiang, D. E. Global minimization of gold clusters by combining neural network potentials and the basin-hopping method. *Nanoscale* **2015**, *7*, 14817–14821.
- (50) Hamad, S.; Catlow, C. R. A.; Woodley, S. M.; Lago, S.; Mejias, J. A. Structure and stability of small TiO₂ nanoparticles. *J. Phys. Chem. B* **2005**, *109*, 15741–15748.
- (51) Lv, J.; Wang, Y. C.; Zhu, L.; Ma, Y. M. Particle-swarm structure prediction on clusters. *J. Chem. Phys.* **2012**, *137*, 084104.
- (52) Zhang, Y. X.; Yang, Z. X. Tuning the catalytic activity of Ag-Pd alloy cluster for hydrogen dissociation by controlling the Pd ratio. *Comput. Theor. Chem.* **2015**, *1071*, 39–45.
- (53) Zhao, J. J.; Xie, R. H. Genetic Algorithms for the Geometry Optimization of Atomic and Molecular Clusters. *J. Comput. Theor. Nanosci.* **2004**, *1*, 117–131.
- (54) Lloyd, L. D.; Johnston, R. L.; Roberts, C.; Mortimer-Jones, T. V. Geometry optimization of aluminium clusters using a genetic algorithm. *ChemPhysChem* **2002**, *3*, 408–415.
- (55) Johnston, R. L. Evolving better nanoparticles: Genetic algorithms for optimizing cluster geometries. *Dalton Trans.* **2003**, 4193–4207.
- (56) Plimpton, S. Fast Parallel Algorithms for Short-Range Molecular-Dynamics. *J. Comput. Phys.* **1995**, *117*, 1–19.
- (57) Chuang, F. C.; Liu, B.; Wang, C. Z.; Chan, T. L.; Ho, K. M. Global structural optimization of Si magic clusters on the Si(111) 7 × 7 surface. *Surf. Sci.* **2005**, *598*, L339–L346.
- (58) Albe, K.; Nordlund, K.; Averback, R. S. Modeling the metal-semiconductor interaction: Analytical bond-order potential for platinum-carbon. *Phys. Rev. B: Condens. Matter Mater. Phys.* **2002**, *65*, 195124.
- (59) Tersoff, J. Empirical Interatomic Potential for Carbon, with Applications to Amorphous-Carbon. *Phys. Rev. Lett.* **1988**, *61*, 2879–2882.
- (60) Kresse, G.; Furthmuller, J. Efficiency of ab-initio total energy calculations for metals and semiconductors using a plane-wave basis set. *Comput. Mater. Sci.* **1996**, *6*, 15–50.
- (61) Kresse, G.; Furthmuller, J. Efficient iterative schemes for ab initio total-energy calculations using a plane-wave basis set. *Phys. Rev. B: Condens. Matter Mater. Phys.* **1996**, *54*, 11169–11186.
- (62) Blochl, P. E. Projector Augmented-Wave Method. *Phys. Rev. B: Condens. Matter Mater. Phys.* **1994**, *50*, 17953–17979.
- (63) Kresse, G.; Joubert, D. From ultrasoft pseudopotentials to the projector augmented-wave method. *Phys. Rev. B: Condens. Matter Mater. Phys.* **1999**, *59*, 1758–1775.
- (64) Perdew, J. P.; Burke, K.; Wang, Y. Generalized gradient approximation for the exchange-correlation hole of a many-electron system. *Phys. Rev. B: Condens. Matter Mater. Phys.* **1996**, *54*, 16533–16539.
- (65) Perdew, J. P.; Burke, K.; Ernzerhof, M. Generalized gradient approximation made simple. *Phys. Rev. Lett.* **1996**, *77*, 3865–3868.
- (66) Perdew, J. P.; Yue, W. Accurate and Simple Density Functional for the Electronic Exchange Energy - Generalized Gradient Approximation. *Phys. Rev. B: Condens. Matter Mater. Phys.* **1986**, *33*, 8800–8802.
- (67) Longo, R. C.; Gallego, L. J. Structures of 13-atom clusters of fcc transition metals by ab initio and semiempirical calculations. *Phys. Rev. B: Condens. Matter Mater. Phys.* **2006**, *74*, 193409.
- (68) Chang, C. M.; Chou, M. Y. Alternative low-symmetry structure for 13-atom metal clusters. *Phys. Rev. Lett.* **2004**, *93*, 133401.
- (69) Wang, L. L.; Johnson, D. D. Density functional study of structural trends for late-transition-metal 13-atom clusters. *Phys. Rev. B: Condens. Matter Mater. Phys.* **2007**, *75*, 235405.
- (70) Li, L.; Larsen, A. H.; Romero, N. A.; Morozov, V. A.; Glinzvad, C.; Abild-Pedersen, F.; Greeley, J.; Jacobsen, K. W.; Norskov, J. K. Investigation of Catalytic Finite-Size-Effects of Platinum Metal Clusters. *J. Phys. Chem. Lett.* **2013**, *4*, 222–226.
- (71) Toyoda, E.; Jinnouchi, R.; Hatanaka, T.; Morimoto, Y.; Mitsuhashi, K.; Visikovskiy, A.; Kido, Y. The d-Band Structure of Pt Nanoclusters Correlated with the Catalytic Activity for an Oxygen Reduction Reaction. *J. Phys. Chem. C* **2011**, *115*, 21236–21240.
- (72) Liu, X.; Sui, Y. H.; Duan, T.; Meng, C. G.; Han, Y. CO oxidation catalyzed by Pt-embedded graphene: a first-principles investigation. *Phys. Chem. Chem. Phys.* **2014**, *16*, 23584–23593.
- (73) Li, Y. F.; Zhou, Z.; Yu, G. T.; Chen, W.; Chen, Z. F. CO Catalytic Oxidation on Iron-Embedded Graphene: Computational Quest for Low-Cost Nanocatalysts. *J. Phys. Chem. C* **2010**, *114*, 6250–6254.
- (74) Ramos-Sanchez, G.; Balbuena, P. B. Interactions of platinum clusters with a graphite substrate. *Phys. Chem. Chem. Phys.* **2013**, *15*, 11950–11959.
- (75) Norskov, J. K.; Bligaard, T.; Rossmeisl, J.; Christensen, C. H. Towards the computational design of solid catalysts. *Nat. Chem.* **2009**, *1*, 37–46.
- (76) Kim, G.; Kawazoe, Y.; Lee, K. R. Controlled Catalytic Properties of Platinum Clusters on Strained Graphene. *J. Phys. Chem. Lett.* **2012**, *3*, 1989–1996.
- (77) Bader, R. F. W. A Quantum-Theory of Molecular-Structure and Its Applications. *Chem. Rev.* **1991**, *91*, 893–928.
- (78) Henkelman, G.; Arnaldsson, A.; Jonsson, H. A fast and robust algorithm for Bader decomposition of charge density. *Comput. Mater. Sci.* **2006**, *36*, 354–360.

(79) Glendening, E. D.; Landis, C. R.; Weinhold, F. Natural bond orbital methods. *Wires Comput. Mol. Sci.* **2012**, *2*, 1–42.

(80) Dunnington, B. D.; Schmidt, J. R. Generalization of Natural Bond Orbital Analysis to Periodic Systems: Applications to Solids and Surfaces via Plane-Wave Density Functional Theory. *J. Chem. Theory Comput.* **2012**, *8*, 1902–1911.